PROCEEDINGS OF SCIENCE

Update of the Helium flux measurement with CALET on the International Space Station

Paolo Brogi,[a,b,*] **K. Kobayashi**[c,d] **and M. Mattiazzi**[e,f] **for the CALET collaboration**

[a] *INFN Sezione di Pisa,*
Polo Fibonacci, Largo B. Pontecorvo, 3, 56127 Pisa, Italy
[b] *Department of Physical Sciences, Earth and Environment, University of Siena,*
via Roma 56, 53100 Siena, Italy
[c] *Waseda Research Institute for Science and Engineering, Waseda University,*
17 Kikuicho, Shinjuku, Tokyo 162-0044, Japan
[d] *Space Environment Utilization Center, Human Spaceflight Technology Directorate,*
Japan Aerospace Exploration Agency, 2-1-1 Sengen, Tsukuba, Ibaraki 305-8505, Japan
[e] *Department of Physics and Astronomy, University of Padova,*
Via Marzolo, 8, 35131 Padova, Italy
[f] *INFN Sezione di Padova,*
Via Marzolo, 8, 35131 Padova, Italy

E-mail: paolo.brogi@unisi.it

The CALorimetric Electron Telescope (CALET) is a space-based calorimetric instrument, designed to carry out precise measurements of high energy cosmic rays. Installed on the Japanese Experiment Module – Exposed Facility on the ISS, it is collecting data with excellent performance and no significant interruptions since October 2015. We present the updated results of the direct measurement of the energy spectrum of cosmic-ray helium, based on more than 9 years of collected data, with an expected statistical increase of about 40% compared with the previously published measurement. The helium flux shows significant deviations from a single power law with a progressive hardening around a few hundred GeV followed by a softening in the multi-TeV region. The increase in statistics allows to extend the upper limit of the measured energy range and to improve the precision of the measurement itself in the high energy part of the spectrum.

39th International Cosmic Ray Conference (ICRC2025)
15–24 July 2025
Geneva, Switzerland

*Speaker

PoS(ICRC2025)019

1. Introduction

The CALorimetric Electron Telescope (CALET) is a space-based experiment developed and operated by an international collaboration led by the Japanese Aerospace Exploration Agency (JAXA) with the participation of the Italian Space Agency (ASI) and NASA. The CALET detector was installed on the Japanese Experiment Module Exposed Facility (JEM-EF) onboard the International Space Station (ISS) since August 2015, and after a preliminary commissioning phase, it is taking data smoothly from October 2015.
The observation of spectral features departing from a single power law in the energy spectra operated by several experiments are not easily accommodated within the conventional models of Galactic cosmic-ray acceleration and propagation. Prompting new theoretical interpretations in terms of revised acceleration and propagation mechanisms, as well as the possible contribution of local sources in the injection spectra of Galactic cosmic rays. Therefore, accurate measurements of the high-energy spectra of individual elements and of their flux ratios are of particular interest and can provide additional discrimination power among the proposed theoretical models and improve our understanding of CR origin. In this paper, we present an update of the Helium flux measurement (already published in Ref. [1]). The presented results are based on the data collected in 3368 days (> 9 years) of CALET operation onboard the ISS, with an expected statistical increase of about 40% with respect to the already published data.

2. The CALET telescope

The CALET main telescope is an all-calorimetric instrument that consists of three sub-detectors. The CHarge Detector (CHD), that is positioned at the top of the apparatus and consists of a two layer hodoscope of plastic scintillators paddles (14 paddles for each layer): this first sub-detector performs the charge identification of individual nuclear species, providing a measurement of the charge Z of the incident particle over a wide dynamic range (from $Z = 1$ up to $Z = 40$). The IMaging Calorimeter (IMC) is a fine grained sampling calorimeter segmented longitudinally into 16 layers of scintillating fibers (with 1 mm^2 square cross-section) read out individually and arranged in pairs along orthogonal directions. Each pair is interleaved with thin tungsten absorbers (for a total thickness of $3X_0$). It is used to reconstruct the early shower profile and the impinging particle trajectory with good angular resolution and a redundant charge measurement [2]. The third detector is the Total AbSorption Calorimeter (TASC), an homogeneous calorimeter made of 12 layers of lead-tungstate (PWO) logs, arranged in pairs along $x - y$ directions, and capable, with its 27 X_0 thickness and its shower imaging capability, to measure electrons and gamma-rays with an excellent energy resolution, providing high discrimination against hadronic cascades.
The total thickness of the main telescope is equivalent to 30 X_0 and 1.3 proton interaction lengths (λ_I), the geometrical factor is 0.12 m^2 sr. A more detailed description of the instrument can be found in Ref. [3] and in the Supplemental Material (SM) of Ref. [4].

3. Data analysis

In the analysis reported here, we use 3368 days of flight data (FD) collected from October 13, 2015 to December 31, 2024. The raw signal of each detector channel is carefully calibrated using

penetrating protons and He particles, selected in-flight by a dedicated trigger mode in order to correct for non-uniformity in light output, gain differences among the channels, position, temperature and temporal gain variations [3]. For each CR event the impinging particle track, charge and energy are then reconstructed. This allows for selection of the helium sample, sorted into energy intervals, in order to compute the energy spectrum. Detailed Monte Carlo (MC) simulations based on EPICS, FLUKA and Geant4 [5] packages were developed. They are used to validate and tune the reconstruction method and evaluate event reconstruction efficiencies, background contaminations and the energy response matrix. The whole analysis is carefully described here [1], in the following subsections we report the main steps of the procedure.

3.1 Preselection

Well reconstructed and contained events were selected on the basis of the following criteria: **Trigger:** the on-board high-energy (HE) trigger mode, used for this analysis, is designed to ensure maximum exposure to electrons above 10 GeV and other high-energy shower events. An offline trigger confirmation is applied, requiring sufficiently more severe conditions than the HE trigger to avoid position, temperature and temporal gain variations. **Track quality cut:** only well reconstructed trucks using a combinatorial Kalman Filter (KF) algorithm [6] are selected. A minimum number of points are required for each track segment, and a χ^2 cut is applied. For He nuclei we achieve an angular resolution of about 0.1°and a resolution on the CHD of ~400 μm. **Geometrical condition:** The reconstructed events are required to pass through the whole detector, i.e., from CHD top to TASC bottom, with 2 cm clearance from the edges of the TASC top layer. Within a fiducial region, known as acceptance A1, limited to a Geometric Factor of 0.051 $m^2 sr$ (~49% of the total GF). **Electron rejection:** This cut is based on the energy deposits found inside one Moliere radius around each IMC fiber matched to the track and on the energy deposit in the last TASC layer. Most of the electrons are rejected while retaining a very high efficiency for helium nuclei (> 99.9% for $E > 50$ GeV). **Off-Acceptance Rejection (OAR) cuts:** Due to the occasional misidentification of one of the secondary tracks as the primary track a number of events are erroneously reconstructed inside the fiducial acceptance A1, while the true acceptance is different. To reject most of these events, different topological cuts are applied using the TASC information.

3.2 Charge identification

In CALET, the charge is measured with two independent subsystems that are routinely used to cross-calibrate each other: the CHD and the IMC. The tracking information is used to select the CHD paddles crossed by the primary particle, the information from the two CHD layers is combined into a single charge estimator. The IMC, being equipped with individually readout scintillating fibers, has a suitable granularity not only to provide excellent tracking capabilities, but also to sample the ionization deposits along the track in each layer, providing an alternative charge estimator through multiple dE/dx measurement. Both charge measurements are calibrated and corrected for several effects: position, time-dependence, non-linear response due to the saturation of the scintillation light, energy shift related to the back-splash background increasing with energy. Then, to have a perfect agreement between the flight data (FD) and MC, the MC data are fine tuned over FD. An energy dependent charge cut, on both charge estimators, is used to select the Helium

nuclei among the other nuclear species. This allows for an almost flat charge selection efficiency (roughly 65%). See Ref. [1] and its SM for details.

3.3 Background subtraction

Background contamination is estimated from the MC simulation of protons and helium, and from FD, as a function of the observed energy. Available spectral data, e.g. from Refs. [7–9], are used to simulate their spectral shape. The MC simulations are used to evaluate the relative contributions, and the FD to assess the proton and helium relative abundances. The dominant component is the charge contamination from protons misidentified as helium. Other non-negligible contributions are from off-acceptance events mis-reconstructed inside acceptance A1. The estimated background is then subtracted bin by bin from the measured helium candidate distribution (dN/dE), prior to the unfolding procedure used to reconstruct the primary particle energy starting from the measured shower energy in TASC.

3.4 Energy measurement

The shower energy of each event is calculated as the sum of the calibrated energy deposits of all the TASC channels. Unlike for electrons, the energy released in TASC by interacting CR nuclei is only a fraction of the primary particle energy with large event-to-event fluctuations. For flux measurement, energy unfolding is applied by means of an iterative unfolding method based on the Bayes theorem [10], to correct dN/dE distribution of selected helium candidates for significant bin-to-bin migration effects (due to the limited energy resolution) and infer the primary particle energy. The energy bin width is chosen commensurate with the RMS resolution of TASC (30% for nuclei).

3.5 Systematic evaluation

The sources of systematic uncertainties in helium analysis can be grouped into energy independent and energy dependent contributions. The former include systematic effects in normalization that were studied in details here [4] and is estimated as 4.1%. The latter includes the following contributions: trigger, shower energy correction, track and acceptance reconstruction, background subtraction, unfolding, charge ID and off-acceptance rejection cuts, MC model. A detailed explanation of the systematic uncertainties evaluation can be found in [1] and its SM. In the present work we have performed a more detailed evaluation of the systematic uncertainty related to the MC model using two alternative Monte Carlo (i.e. Fluka and Geant4) to compare with the adopted one (EPICS), while in the past only Fluka was used. More in details, the systematic error is obtained for each bin using Fluka or Geant4 instead of EPICS to evaluate: the shower energy correction, the smearing matrix, and all relevant selection efficiencies. In Fig, 1 a breakdown of the systematic uncertainties is represented.

4. Helium energy spectrum and p/He ratio

The helium energy spectrum is calculated as: $\Phi(\tilde{E}) = \dfrac{N(E)}{\Delta E \times \varepsilon(E) \times \Omega \times LT}$ where $\tilde{E}$ is the median kinetic energy of the $[E, E + \Delta E)$ bin, ΔE is the energy bin width, $\varepsilon(E)$ the overall selection

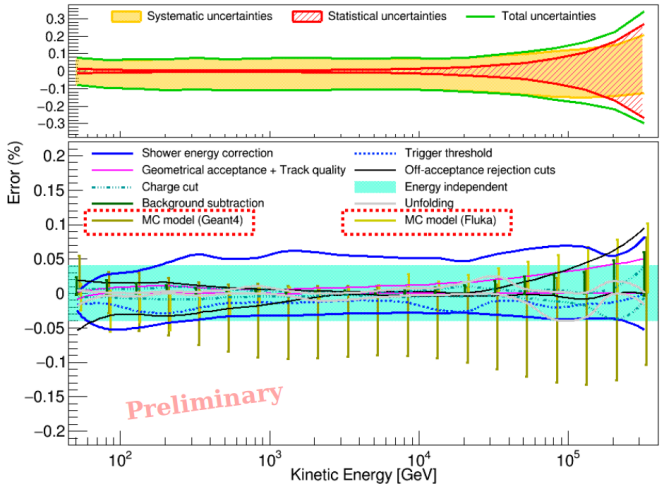

Figure 1: Breakdown of the systematic uncertainties evaluated in this analysis. Each colored line represent a different systematic, the total systematic error is shown by the solid green band. The red hatched area represent the statistical error.

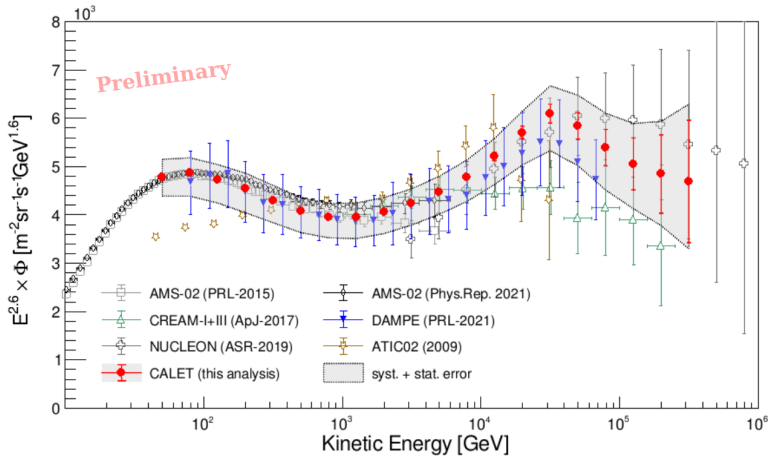

Figure 2: Helium flux measurement with CALET (red markers), compared with previous direct observations [8, 9, 11–14]. The error bars represent only the statistical error; the gray band represents the quadratic sum of statistical and systematic error. The light violet colored band shows the systematic uncertainty of [14].

efficiency, and LT is the live time ($\sim$ 85% of total observation time), Ω the "fiducial" geometrical acceptance ($\sim$ 510 $cm^2 sr$), $N(E)$ the bin content in the unfolded distribution.

The energy spectrum of helium nuclei in CR, as measured by CALET with this analysis in 3368 days of operation, is shown in Fig. 2 covering an interval of kinetic energy per particle from ~40 GeV to ~400 TeV, compared with previous observations from space-based [9, 11–14] and balloon-borne [8] experiments. Our spectrum is in good agreement with the very accurate measurements by AMS-02 in the lower energy region below a few TeV, as well as with the measurements from

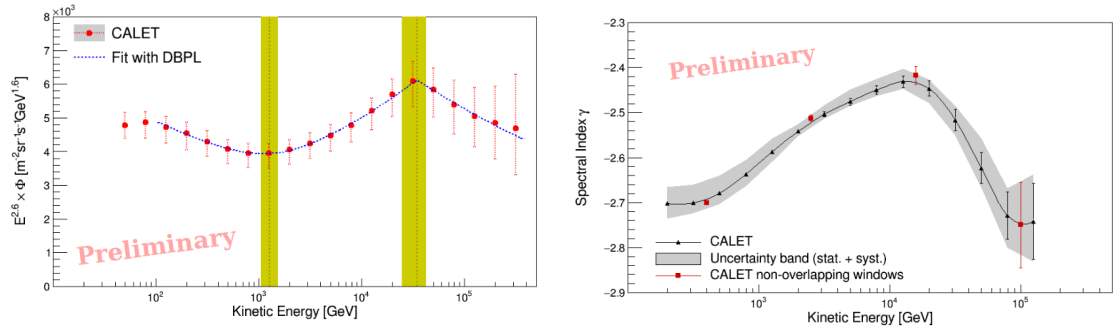

Figure 3: Left panel: fit of CALET data with a DBPL function [1]. Both statistical and systematic uncertainties are taken into account. Right panel: energy dependence of the spectral index calculated within a sliding energy window for CALET data. The gray band indicates the uncertainty range including systematics. The red marker indicates the spectral index calculated within 4 bins wide non-overlapping sliding energy windows.

calorimetric instruments in the higher energy region, in particular with the recent measurement of DAMPE [14]. A fit of CALET data has been performed using a "double smoothly broken power-law" as described in Ref. [1], in the energy range from 100 GeV to 400 TeV, and is reported in the left panel of Fig. 3. A progressive hardening up to the multi-TeV region was observed, and the fit gives a power law index (γ), $\Delta\gamma$ and break energy (E_0) consistent, within the errors, with other experimental results like [14]. A progressive hardening from a few hundred GeV to a few tens TeV and the onset of a flux softening above a few tens of TeV are observed. The fit returns a power law index $\gamma = -2.72\,^{+0.01}_{-0.01}\,(stat)\,^{+0.03}_{-0.03}\,(syst)$, $\Delta\gamma = 0.29\,^{+0.03}_{-0.02}\,(stat)\,^{+0.07}_{-0.04}\,(syst)$, first break energy $E_0 = 1276\,^{+111}_{-94}\,(stat)\,^{+250}_{-198}\,(syst)$ GeV and smoothness parameter $S = 2.0\,^{+0.4}_{-0.4}\,(stat)\,^{+1.8}_{-1.0}\,(syst)$, with a second spectral index variation $\Delta\gamma_1 = -0.31\,^{+0.07}_{-0.09}\,(stat)\,^{+0.06}_{-0.08}\,(syst)$ and second break energy $E_1 = 34.6\,^{+7.2}_{-5.5}\,(stat)\,^{+1.6}_{-6.1}\,(syst)$ TeV. Given the relatively large uncertainties of the data in the highest energy bins, the second smoothness parameter $S_1 = 114\,^{+83}_{-109}\,(stat)\,^{+194}_{-103}\,(syst)$ cannot be effectively constrained. The fit parameters are generally consistent, within the errors, with the previously published CALET results [1] and DAMPE results [14]. The spectral hardening and softening can be easily seen also in the right panel of Fig. 3, where the spectral index is shown as a function of kinetic energy. The black marker in the plot represents the index γ with its statistical error, while the gray band represents the quadratic sum of statistical end systematic uncertainties. The superimposed red marker indicates the spectral index calculated within 4 bins wide not overlapping sliding energy windows. Differences between the proton and helium spectra can contribute important constraints on acceleration models. Since usually acceleration mechanism are considered rigidity dependent, and also to ease the comparison with other previous measurements, we have calculated the proton over He flux ratio in rigidity. To do that, the helium spectrum (from this analysis) and the proton spectrum (from Ref. [16]) has been computed in rigidity (following the same procedure reported in the SM of Ref. [1]) and then the proton over He flux ratio has been derived. The ^{3}He contribution to the flux has been taken into account assuming the AMS-02 [17] measurement of the ^{3}He/^{4}He ratio and extrapolating it to higher energies with use of a single power-law fit. The p/He flux ratio shown in the right panel of Fig. 4, has been measured by CALET with high statistical precision,

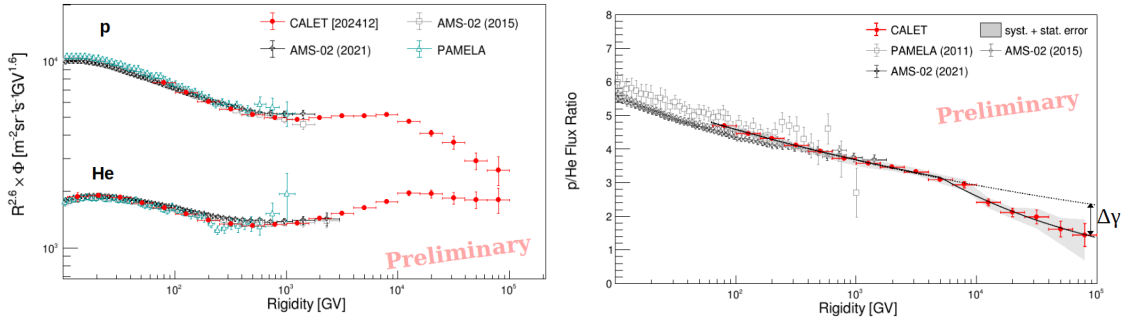

Figure 4: p/He ratio measurement with CALET (red markers), compared with previous direct observations [9, 13, 15]. The error bars represent only statistical error, the gray band represents statistical and systematic error.

in a wide energy range from 60 GV to 100 TV. Both the statistical (red bars) and the sum of statistical and systematic errors (gray band) are represented. Details on the measurement and the systematic uncertainty calculation can be found in Ref. [1] and its SM. Measurements from other experiments [9, 13, 15] are also included in the same plot. The measured p/He flux ratio results well described by a single power law (PL) function $\Phi(R) = A \cdot R^{\gamma}$ from tens of GV up to 10 TV (black dashed line in Fig. 4), while significantly deviating above. The solid black line in the right plot of Fig. 4 shows a fit with a double power law (DPL) function

$$\Phi(R) = \begin{cases} C\left(\frac{R}{GV}\right)^{\gamma} & R < R_0 \\ C\left(\frac{R}{GV}\right)^{\gamma}\left(\frac{R}{R_0}\right)^{\Delta\gamma} & R > R_0 \end{cases}$$

performed from 60 GV up to 100 TV. In this energy range a DPL is favored, and a PL is excluded with a significance of 4.8 σ including systematic error. The fit returns a power law index $\gamma = -0.097 \pm 0.006$ and a $\Delta\gamma = -0.23 \pm 0.08$, with $R_0 = 6.6 \pm 1.9$ TV.

5. Conclusions

The measurement of the helium spectrum demonstrates the excellent capability of CALET to resolve spectral features in the CR spectra in the large energy range from 40 GeV to 250 TeV. The spectral shape is not consistent with a single power law, confirms the presence of a hardening above a few hundred GeV, and a flux softening above a few tens TeV. A DBPL fits both spectral features with parameters that are found to be consistent, within the errors, with the most recent results of DAMPE [14]. We have also measured the p/He ratio in the interval from 60 GV to 100 TV. Our result extends the energy reach with spectrometers by about two orders of magnitude, and is found to be in substantial agreement with previous measurements [9, 15] up to 10 TV, although it does not show any hint of flattening at intermediate energies as reported in [13]. However, above 10 TV it clearly shows a deviation from a single power law with a significance of 4.8σ, reflecting the fact that flux softening appears to be more pronounced in protons than in helium.

6. Acknowledgments

We gratefully acknowledge JAXA's contributions to the development of CALET and to the operations aboard the JEM-EF on the ISS. This work was supported in part by JSPS Grant-in-Aid for Scientific Research (S) No. 26220708, No. 19H05608, and No. 24H00025, JSPS Grant-in-Aid for Scientific Research (B) No. 24K00665, and by the MEXT Supported Program for the Strategic Research Foundation at Private Universities (2011-2015) (No. S1101021) at Waseda University. The CALET effort in Italy is supported by ASI under Agreement No. 2013-018-R.0 and its amendments. The CALET effort in the United States is supported by NASA through Grants No. NNX16AB99G, No. NNX16AC02G, and No. NNH14ZDA001N-APRA-0075.

References

[1] O. Adriani et al. (CALET Collab.), Phys. Rev. Lett. **130**, 171002 (2023).

[2] P. Brogi et al. for the CALET Collaboration , PoS (ICRC2015) 595 (2015)

[3] Y. Asaoka et al. (CALET Collab.), Astropart. Phys. **91**, 1 (2017).

[4] O. Adriani et al. (CALET Collab.), Phys. Rev. Lett. **119**, 181101 (2017).

[5] K. Kasahara, Proc. of 24 th ICRC, Vol. 1 (1995) 399, T. T. Böhlen et al., Nuclear Data Sheets 120 (2014) 211 and S. Agostinelli et al. NIM-A 5**506**, 3 (2003)

[6] P. Maestro and N. Mori (for the CALET Collab.), PoS (ICRC2017) 208 (2017).

[7] M. Aguilar et al. (AMS Collab.), Phys. Rev. Lett. **114**, 171103 (2015).

[8] Y. S. Yoon et al., Astrophys. J. **728**, 122 (2011); Astrophys. J. **839**, 5 (2017).

[9] M. Aguilar et al. (AMS Collab.), Phys. Rev. Lett. **115**, 211101 (2015).

[10] G. D'Agostini, NIM-A 362 (1995) 487 and T. Adye, arXiv:1105.1160v1 (2011)

[11] A.D. Panov et al., Bull. Russian Acad. Sci. 73, 564 (2009)

[12] V. Grebenyuk et al., ASR 64, 2546 (2019)

[13] M. Aguilar et al., Phys. Rep. 894, 1 (2021)

[14] F. Alemanno et al. (DAMPE Collab.), Phys. Rev. Lett. **126**, 201102 (2021).

[15] O. Adriani et al., Science **332**, 69 (2011).

[16] K. Kobayashi and P.S. Marrocchesi for the CALET Collaboration PoS(ICRC2025)150.

[17] M. Aguilar et al. (AMS Collab.), Phys. Rev. Lett. **123**, 181102 (2019).

Full Author List: CALET Collaboration

O. Adriani[1,2], Y. Akaike[3,4], K. Asano[5], Y. Asaoka[5], E. Berti[2,6], P. Betti[2,6], G. Bigongiari[7,8], W.R. Binns[9], M. Bongi[1,2], P. Brogi[7,8], A. Bruno[10], N. Cannady[11], G. Castellini[6], C. Checchia[7,8], M.L. Cherry[12], G. Collazuol[13,14], G.A. de Nolfo[10], K. Ebisawa[15], A.W. Ficklin[12], H. Fuke[15], S. Gonzi[1,2,6], T.G. Guzik[12], T. Hams[16], K. Hibino[17], M. Ichimura[18], M.H. Israel[9], K. Kasahara[19], J. Kataoka[20], R. Kataoka[21], Y. Katayose[22], C. Kato[23], N. Kawanaka[24,25], Y. Kawakubo[26], K. Kobayashi[3,4], K. Kohri[25,27], H.S. Krawczynski[9], J.F. Krizmanic[11], P. Maestro[7,8], P.S. Marrocchesi[7,8], M. Mattiazzi[13,14], A.M. Messineo[8,28], J.W. Mitchell[11], S. Miyake[29], A.A. Moiseev[11,30,31], M. Mori[32], N. Mori[2], H.M. Motz[33], K. Munakata[23], S. Nakahira[15], J. Nishimura[15], M. Negro[12], S. Okuno[17], J.F. Ormes[34], S. Ozawa[35], L. Pacini[2,6], P. Papini[2], B.F. Rauch[9], S.B. Ricciarini[2,6], K. Sakai[36], T. Sakamoto[26], M. Sasaki[11,30,31], Y. Shimizu[17], A. Shiomi[37], P. Spillantini[1], F. Stolzi[7,8], S. Sugita[26], A. Sulaj[7,8], M. Takita[5], T. Tamura[17], T. Terasawa[5], S. Torii[3], Y. Tsunesada[38,39], Y. Uchihori[40], E. Vannuccini[2], J.P. Wefel[12], K. Yamaoka[41], S. Yanagita[42], A. Yoshida[26], K. Yoshida[19], and W.V. Zober[9]

[1]Department of Physics, University of Florence, Via Sansone, 1 - 50019, Sesto Fiorentino, Italy, [2]INFN Sezione di Firenze, Via Sansone, 1 - 50019, Sesto Fiorentino, Italy, [3]Waseda Research Institute for Science and Engineering, Waseda University, 17 Kikuicho, Shinjuku, Tokyo 162-0044, Japan, [4]Space Environment Utilization Center, Human Spaceflight Technology Directorate, Japan Aerospace Exploration Agency, 2-1-1 Sengen, Tsukuba, Ibaraki 305-8505, Japan, [5]Institute for Cosmic Ray Research, The University of Tokyo, 5-1-5 Kashiwa-no-Ha, Kashiwa, Chiba 277-8582, Japan, [6]Institute of Applied Physics (IFAC), National Research Council (CNR), Via Madonna del Piano, 10, 50019, Sesto Fiorentino, Italy, [7]Department of Physical Sciences, Earth and Environment, University of Siena, via Roma 56, 53100 Siena, Italy, [8]INFN Sezione di Pisa, Polo Fibonacci, Largo B. Pontecorvo, 3 - 56127 Pisa, Italy, [9]Department of Physics and McDonnell Center for the Space Sciences, Washington University, One Brookings Drive, St. Louis, Missouri 63130-4899, USA, [10]Heliospheric Physics Laboratory, NASA/GSFC, Greenbelt, Maryland 20771, USA, [11]Astroparticle Physics Laboratory, NASA/GSFC, Greenbelt, Maryland 20771, USA, [12]Department of Physics and Astronomy, Louisiana State University, 202 Nicholson Hall, Baton Rouge, Louisiana 70803, USA, [13]Department of Physics and Astronomy, University of Padova, Via Marzolo, 8, 35131 Padova, Italy, [14]INFN Sezione di Padova, Via Marzolo, 8, 35131 Padova, Italy, [15]Institute of Space and Astronautical Science, Japan Aerospace Exploration Agency, 3-1-1 Yoshinodai, Chuo, Sagamihara, Kanagawa 252-5210, Japan, [16] Center for Space Sciences and Technology, University of Maryland, Baltimore County, 1000 Hilltop Circle, Baltimore, Maryland 21250, USA, [17]Kanagawa University, 3-27-1 Rokkakubashi, Kanagawa, Yokohama, Kanagawa 221-8686, Japan, [18]Faculty of Science and Technology, Graduate School of Science and Technology, Hirosaki University, 3, Bunkyo, Hirosaki, Aomori 036-8561, Japan, [19]Department of Electronic Information Systems, Shibaura Institute of Technology, 307 Fukasaku, Minuma, Saitama 337-8570, Japan, [20]School of Advanced Science and Engineering, Waseda University, 3-4-1 Okubo, Shinjuku, Tokyo 169-8555, Japan, [21] Okinawa Institute of Science and Technology, 1919-1 Tancha, Onna-son, Kunigami-gun Okinawa 904-0495, Japan, [22]Faculty of Engineering, Division of Intelligent Systems Engineering, Yokohama National University, 79-5 Tokiwadai, Hodogaya, Yokohama 240-8501, Japan, [23]Faculty of Science, Shinshu University, 3-1-1 Asahi, Matsumoto, Nagano 390-8621, Japan, [24]Department of Physics, Graduate School of Science, Tokyo Metropolitan University , 1-1 Minamii-Osawa, Hachioji, Tokyo 192-0397, Japan, [25]National Astronomical Observatory of Japan, 2-21-1 Osawa, Mitaka, Tokyo 181-8588, Japan, [26]Department of Physical Sciences, College of Science and Engineering, Aoyama Gakuin University, 5-10-1 Fuchinobe, Chuo, Sagamihara, Kanagawa 252-5258, Japan, [27]Institute of Particle and Nuclear Studies, High Energy Accelerator Research Organization, 1-1 Oho, Tsukuba, Ibaraki 305-0801, Japan, [28]University of Pisa, Polo Fibonacci, Largo B. Pontecorvo, 3 - 56127 Pisa, Italy, [29]Department of Electrical and Electronic Systems Engineering, National Institute of Technology (KOSEN), Gifu College, 2236-2 Kamimakuwa, Motosu-city, Gifu 501-0495, Japan, [30]Center for Research and Exploration in Space Sciences and Technology, NASA/GSFC, Greenbelt, Maryland 20771, USA, [31]Department of Astronomy, University of Maryland, College Park, Maryland 20742, USA, [32]Department of Physical Sciences, College of Science and Engineering, Ritsumeikan University, Shiga 525-8577, Japan, [33]Faculty of Science and Engineering, Global Center for Science and Engineering, Waseda University, 3-4-1 Okubo, Shinjuku, Tokyo 169-8555, Japan, [34]Department of Physics and Astronomy, University of Denver, Physics Building, Room 211, 2112 East Wesley Avenue, Denver, Colorado 80208-6900, USA, [35]Quantum ICT Advanced Development Center, National Institute of Information and Communications Technology, 4-2-1 Nukui-Kitamachi, Koganei, Tokyo 184-8795, Japan, [36]Kavli Institute for Cosmological Physics, The University of Chicago, 5640 South Ellis Avenue, Chicago, IL 60637, USA, [37]College of Industrial Technology, Nihon University, 1-2-1 Izumi, Narashino, Chiba 275-8575, Japan, [38]Graduate School of Science, Osaka Metropolitan University, Sugimoto, Sumiyoshi, Osaka 558-8585, Japan, [39]Nambu Yoichiro Institute for Theoretical and Experimental Physics, Osaka Metropolitan University, Sugimoto, Sumiyoshi, Osaka 558-8585, Japan, [40]National Institutes for Quantum and Radiation Science and Technology, 4-9-1 Anagawa, Inage, Chiba 263-8555, Japan, [41]Nagoya University, Furo, Chikusa, Nagoya 464-8601, Japan, [42]College of Science, Ibaraki University, 2-1-1 Bunkyo, Mito, Ibaraki 310-8512, Japan.

PoS(ICRC2025)019